Special Collection

Deep-Red Luminescent Molybdenum(0) Complexes with Bi- and Tridentate Isocyanide Chelate Ligands

Patrick Herr[+],[a] Alexander Schwab[+],[b] Stephan Kupfer,*[b] and Oliver S. Wenger*[a]

In octahedral complexes, molybdenum(0) has the same $4d^6$ valence electron configuration as ruthenium(II), which is beneficial for establishing energetically low-lying metal-to-ligand charge transfer (MLCT) excited states. Those MLCT states often show luminescence, and they can furthermore undergo photoinduced electron and energy transfer reactions that are of interest in the context of solar energy conversion, sensing, or photocatalysis. Molybdenum is roughly 100 times more abundant than ruthenium, and it seems desirable to increase our fundamental understanding of the photophysical properties of complexes made from non-precious metals. We report here on the luminescence behavior of two new homoleptic molybdenum(0) isocyanide complexes, one with three bidentate, the other with two tridentate chelate ligands. The key novelty is the incorporation of thiophene units into the ligand backbones, causing strongly red-shifted photoluminescence with respect to comparable molybdenum(0) isocyanides with phenylene units in the ligand backbones. Combined experimental and computational studies provide detailed insight into the photophysical properties of this compound class. This work is relevant for the development of new luminescent compounds with possible applications in lighting and sensing, and it complements current research efforts on photoactive complexes with other abundant transition metal and main group elements.

Introduction

The low-spin d^6 valence electron configuration of second- and third-row transition metals can give rise to metal-to-ligand charge transfer (MLCT) excited states, from which luminescence and different types of photo-reactivities can occur. This behavior is typical for many Ru^{II}, Os^{II}, Re^{I} and Ir^{III} complexes,[1] but examples of d^6 MLCT luminophores and photocatalysts with abundant transition metals have remained scarce.[2] First-row transition metals such as iron or manganese are particularly attractive,[3] but whereas relatively long-lived MLCT excited states in Fe^{II} complexes have been successfully installed,[4] this compound class has remained non-emissive until very recently,[5] and their photocatalytic applications seem to rely mostly on (dark) metal-centered excited states.[6] Isoelectronic Mn^{I} shows MLCT luminescence when embedded into hexakis(arylisocyanide) coordination environments, but until now, the luminescence quantum yields are yet very low.[7] The same is true for isoelectronic Cr^0 isocyanide complexes.[8] By contrast, Mo^0 isocyanide complexes can show bright MLCT emission with luminescence quantum yields surpassing that of the prototypical $[Ru(bpy)_3]^{2+}$ compound (bpy = 2,2′-bipyridine).[9] Initial ligand designs were based on a *m*-terphenyl backbone to obtain bidentate chelators,[10] but recently we started focusing on ligands that contain thiophene instead of phenylene spacers in the backbone.[11] This change entails energetically much lower lying MLCT states and substantially red-shifted luminescence.[11] Since a decreased energy gap between the emissive MLCT and the electronic ground state is usually accompanied by a decrease of the luminescence quantum yield (due to enhanced nonradiative excited-state relaxation),[12] it seemed desirable to get more insight into the photophysical properties and electronic structures of Mo^0-based deep-red emitters. Toward this end, we explored the two new complexes in Figure 1 in a joint synthetic-spectroscopic-theoretical approach. The $[Mo(L^{bi})_3]$ complex resembles $[Ru(bpy)_3]^{2+}$ in that it is made from three bidentate ligands, whereas the $[Mo(L^{tri})_2]$ compound is reminiscent of $[Ru(tpy)_2]^{2+}$ (tpy = 2,2′:6′,2″-terpyridine), in which two tridentate ligands coordinate to the metal.[13] However, the photophysical properties of both of these Mo^0 compounds are more similar to $[Os(bpy)_3]^{2+}$ and $[Os(tpy)_2]^{2+}$ in terms of emission color, MLCT excited-state lifetime, and photoluminescence quantum yield.

Obtaining strong MLCT emission from earth-abundant d^6 metal complexes is more difficult than in the case of d^{10} luminophores, owing to metal-centered (MC) excited states that are energetically close to the lowest MLCT state, and which

[a] Dr. P. Herr,[+] Prof. Dr. O. S. Wenger
Department of Chemistry
University of Basel
St. Johanns-Ring 19, 4056 Basel (Switzerland)
E-mail: oliver.wenger@unibas.ch
[b] A. Schwab,[+] Dr. S. Kupfer
Institute of Physical Chemistry
Friedrich Schiller University Jena
Helmholtzweg 4, 07743 Jena (Germany)
E-mail: stephan.kupfer@uni-jena.de
[+] These two authors contributed equally to this work.

Supporting information for this article is available on the WWW under https://doi.org/10.1002/cptc.202200052.

An invited contribution to a Special Collection celebrating the 5 Year Anniversary of ChemPhotoChem.

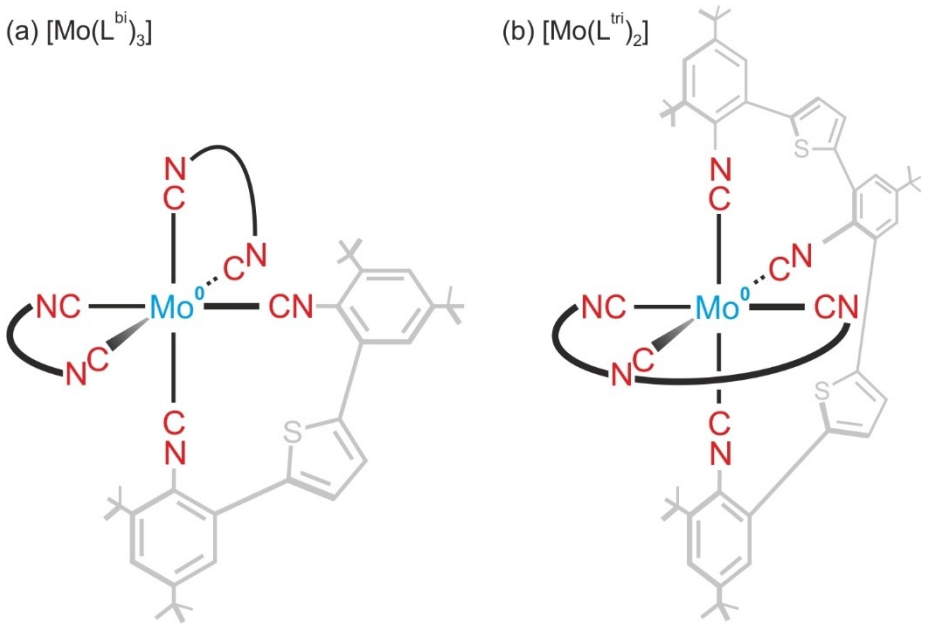

Figure 1. Molecular structures of the two complexes investigated in this work. The bidendate ligand (L^{bi}) is the same as that used for a recent study of an analogous Mn^{I} complex.[7a] The tridentate ligand (L^{tri}) is very similar to that used in the same Mn^{I} study, but differs in the substituent at the central arylisocyanide unit (*tert*-butyl instead of methyl).

can deactivate the MLCT state.[5a,b, 14] In the closed d^{10} subshell, this undesirable relaxation pathway is not available, and consequently the performance factors of d^6 MLCT luminophores based on earth-abundant metals currently still lag much behind those achievable for copper(I) compounds.[15] Analogously, ligand-to-metal charge transfer (LMCT) luminophores based on metals with the d^0 valence electron configuration lack MC states that could negatively affect the emission performance.[16] Furthermore, the MLCT states of d^6 metal luminophores are more strongly distorted than the MC states of d^3 spin-flip emitters such as Cr^{III} polypyridines,[17] in which direct nonradiative relaxation to the electronic ground state is inherently less efficient.[3] This combination of MLCT deactivation channels involving close-by MC states as well as direct relaxation to the electronic ground state (caused by substantial MLCT distortion) poses fundamental challenges for d^6 metal chromophores that we aimed to address in this research. The development of efficient deep-red and near-infrared emitters is generally non-trivial, regardless of whether d^6 MLCT luminophores or other compound classes are considered.[18]

Results and Discussion

Synthesis, Infrared Spectroscopy and Electrochemistry

The $[Mo(L^{bi})_3]$ and $[Mo(L^{tri})_2]$ complexes, Figure 1, were synthesized and characterized as described in the Supporting Information (SI). The ligand L^{bi} was available from a recent investigation of Mn^{I} complexes, whilst L^{tri} is very similar to the tridentate chelate ligand used in the same previous Mn^{I} study, but differs by a *tert*-butyl (instead of a methyl) substituent at the periphery of the central arylisocyanide unit.[7a] Very recently, spectroscopic as well as theoretical studies on the *tert*-butyl *vs.* methyl substituent pattern in structurally closely related bidentate Mo^0 complexes bridged by phenyl spacers showed that excited-state lifetime can be enhanced considerably by sterically demanding substituents (*i.e.*, *tert*-butyl).[19] This way, a full equilibration of the deactivating metal-centered (^{3}MC) states is hampered, see Table S1 in the SI for details. A single isomer with the L^{tri} ligand binding in meridional fashion is obtained for the bis(tridentate) complex, whilst for the tris(bidentate) compound a pair of (Δ and Λ) enantiomers is expectable, but no attempts to separate them were made. The *tert*-butyl substituents at the ligand periphery have no specific function, they are merely present because they are already part of the commercially available 1-bromo-3,5-di-*tert*-butylbenzene starting material.[7a]

The isocyanide C≡N stretching vibrational mode in both free ligands is observed at 2111 cm^{-1}, while its frequency is reduced to 1993 cm^{-1} in $[Mo(L^{bi})_3]$ and 1917 cm^{-1} in $[Mo(L^{tri})_2]$ upon coordination to Mo^0. This observation is in line with previous studies of Mo^0 isocyanides,[9–10,11, 20] as well as with the quantum chemical results obtained in the present joint synthetic-spectroscopic-theoretical study (see Table S2). The decrease in the C≡N vibrational frequency by 118–194 cm^{-1} is a manifestation of substantial π-backbonding (149-169 cm^{-1} predicted by DFT), as often observable for isocyanide complexes with electron-rich metals,[21] see molecular frontier orbitals in Table S3.

Electrochemical oxidation of Mo^0 to Mo^{I} in deaerated THF is reversible in both complexes (Figure 2) and occurs at -0.05 V vs SCE in $[Mo(L^{bi})_3]$ and at 0.0 V vs SCE in $[Mo(L^{tri})_2]$. These low oxidation potentials are very similar to those reported

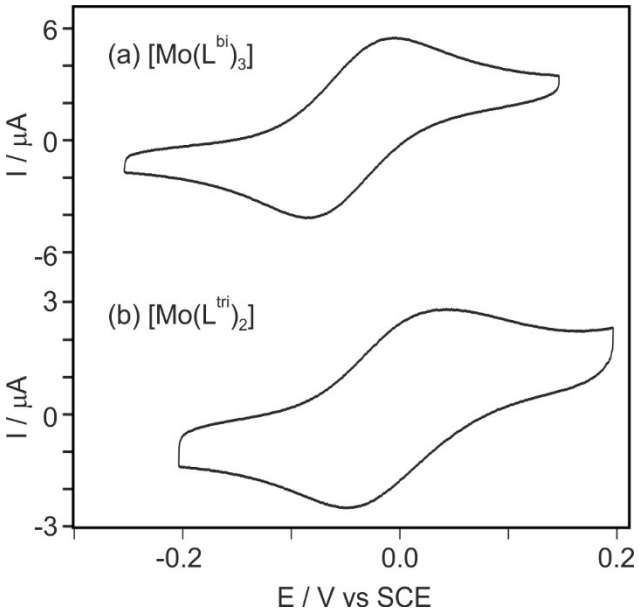

Figure 2. Cyclic voltammograms of the two complexes recorded in dry THF containing 0.25 M $^{n}Bu_4PF_6$ at potential scan rates of 0.3 V/s. Potentials of −0.05 and 0.0 V vs SCE are extracted from these data for the $Mo^{I/0}$ redox couple in $[Mo(L^{bi})_3]$ and $[Mo(L^{tri})_2]$, respectively.

previously for other hexakis(arylisocyanide) complexes of Mo^0 including both monodentate and chelating ligand variants.[9–10,11, 22] The analogous d^6/d^5 oxidation process in $[Ru(bpy)_3]^{2+}$ (in that case corresponding to the Ru^{III}/Ru^{II} couple) occurs at 1.2 V more positive potential,[23] further highlighting the very high electron density at Mo^0. Reductive sweeps in cyclic voltammetry reveal a series of irreversible waves below −2.2 V vs SCE that cannot be unambiguously assigned (Figure S1), but it seems plausible that those waves are associated with ligand-centered reduction processes based on recent studies of Mn^{I} complexes with similar ligands.[7a]

UV/Vis, Luminescence and Transient Absorption Spectroscopy

MLCT bands dominate the absorption properties of $[Mo(L^{bi})_3]$ and $[Mo(L^{tri})_2]$ in the visible spectral range (black traces in Figure 3), particularly between 500 and ca. 700 nm. Both compounds furthermore exhibit a prominent band in the blue spectral range (393 nm for $[Mo(L^{bi})_3]$; 448 nm for $[Mo(L^{tri})_2]$), which is mainly attributable to higher-lying MLCT and intra-ligand charge transfer (ILCT) excitations according to our quantum chemical simulations performed at the time-dependent density functional level of theory (TDDFT). At wavelengths shorter than 350 nm, the UV-Vis spectra of both complexes are dominated by ligand-centered electronic transitions. More detailed band assignments based on computational results follow below.

Following excitation into the MLCT absorption bands at 620 nm, both complexes emit in deaerated THF (red traces in Figure 3) and toluene (Figure S2) at 20 °C. The solvatochromic blue-shift by ca. 400 cm^{-1} of the emission band maximum (λ_{em}) in both complexes when going from THF to the more apolar toluene (Table 1) is in line with the presumed charge-transfer character of the emission. In full agreement, DFT calculations allow to assign the nature of the lowest triplet state unambiguously to be of ^{3}MLCT character in both complexes, see spin density for T_1 in Figure 4. Excitation spectra detected at the respective emission band maxima (blue dotted traces in Figure 3) resemble the MLCT absorption bands of both complexes, and thereby confirm that the photoluminescence is indeed originating from the Mo^0 compounds rather than from any emissive impurities. At wavelengths shorter than 500 nm, the excitation spectra deviate from the absorption spectra, possibly due to less efficient population of the emissive excited state upon irradiating into the electronic transitions absorbing in this spectral range. Luminescence quantum yield (ϕ) measurements were performed using $[Ru(bpy)_3](PF_6)_2$ in aerated acetonitrile as reference[24] following a recently reported

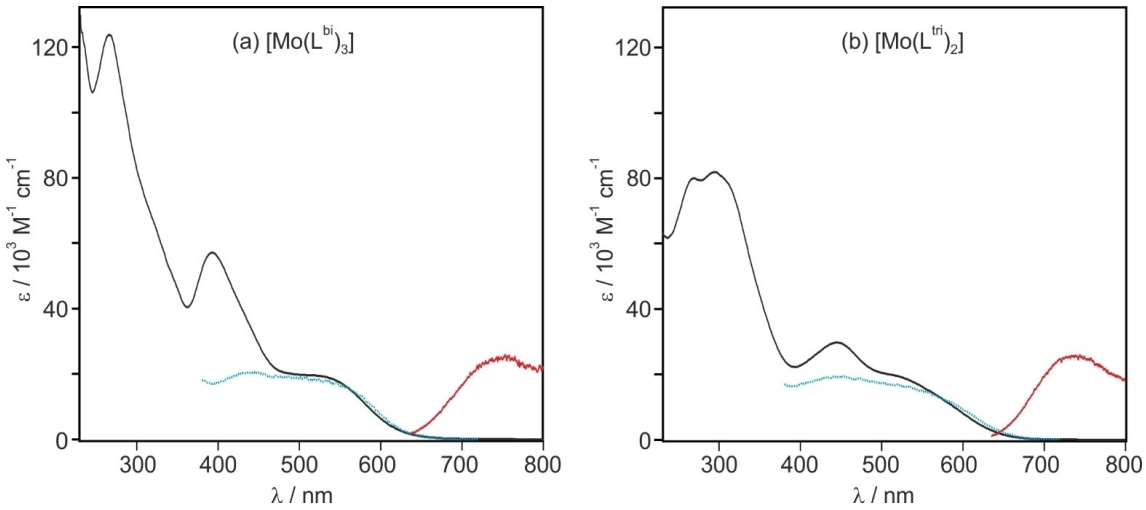

Figure 3. UV/Vis absorption (black), photoluminescence (red), and excitation spectra (blue) recorded in deaerated THF at 20 °C. Excitation occurred at 620 nm (for luminescence spectroscopy), detection at 740 nm (for excitation spectroscopy).

Table 1. Luminescence band maxima (λ_{em}), excited-state lifetimes (τ), and luminescence quantum yields (ϕ) in deaerated solvents under argon at 20 °C. Simulated luminescence wavelengths, obtained by ground state calculations at the density functional level of theory (ΔSCF) as well as at the time-dependent density functional level of theory, are indicated in parentheses, respectively.

	$[Mo(L^{bi})_3]$		$[Mo(L^{tri})_2]$	
	THF	toluene	THF	Toluene
λ_{em} [nm]	750 (807, 796)	728	740 (836, 820)	722
τ [ns][a]	18	30 (73 %), 83 (27 %)	19	28 (62 %), 77 (38 %)
ϕ [%]	N/A	0.68	N/A	0.70

[a] Values in toluene from bi-exponential fits with weighting factors in parentheses. Weighted average values are 44 ns for $[Mo(L^{bi})_3]$ and 47 ns for $[Mo(L^{tri})_2]$.

methodology.[7a] Compared to the current record-holder Mo^0 isocyanide complex based on a chelating ligand with a *m*-terphenyl backbone ($[Mo(L^{tBu})_3]$) that featured a luminescence quantum yield of 20.3 % in deaerated toluene at 20 °C,[9] the ϕ-values of 0.7 % obtained for $[Mo(L^{bi})_3]$ and $[Mo(L^{tri})_2]$ are low (Table 1). At first glance it seems plausible that this is mostly due to the substantially smaller energy gap between the emissive MLCT state in the new complexes compared to the previously investigated $[Mo(L^{tBu})_3]$ compound,[12] which has its emission band maximum at 583 nm in toluene, compared to 728/722 nm for the new complexes considered here. However, as discussed further below, an additional excited-state decay channel involving a metal-centered excited state seemed more important in $[Mo(L^{bi})_3]$ and $[Mo(L^{tri})_2]$, contributing to the enhanced nonradiative relaxation in those complexes, in addition to the effect described by the energy gap law.[12]

In order to elucidate the electronic transitions underlying the absorption bands of $[Mo(L^{bi})_3]$ and $[Mo(L^{tri})_3]$ at the Franck-Condon point, detailed quantum chemical simulations were performed at the TDDFT level of theory. The simulated UV-Vis spectra are presented alongside the experimental data in Figure 4a/b. A detailed list of the calculated excited state properties discussed can be found in Tables S4 to S7. Based on the computational results, the band at around 550 nm of $[Mo(L^{bi})_3]$ (Figure 4a) can be assigned to mainly three dipole-allowed singlet excitations of MLCT character, namely into S_2, S_5 and S_6 predicted at 567, 544 and 535 nm, respectively. At shorter excitation wavelengths and associated with the experimental absorption feature centered at approximately 400 nm, further four prominent MLCT transition, *i.e.* into S_{10}, S_{13}, S_{26} and S_{27} at 441, 425, 371 and 370 nm, are observed, while an ILCT state (S_{28} at 353 nm) is predicted in addition. In a similar fashion, the visible absorption of $[Mo(L^{tri})_3]$ in the range of 600 to 400 nm (Figure 4b) is mainly attributed to six MLCT excitations, *i.e.* into S_1, S_2, S_7, S_{14}, S_{16} and S_{18} at 559, 559, 510, 448, 447 and 429 nm, see Tables S4 and S5 for details.

Following pulsed excitation at 620 ns, the transient UV-Vis absorption spectra shown as solid black traces in Figure 4c/d were recorded. For both compounds, a bleaching of the MLCT ground state absorption bands is observable, and for $[Mo(L^{tri})_2]$ an excited-state absorption band around 400 nm is detectable. To gain insight into the excited-state relaxation processes, quantum chemical simulations, aiming to model the transient UV-Vis spectra of $[Mo(L^{bi})_3]$ and $[Mo(L^{tri})_2]$ upon 620-nm excitation were performed. Hereby, contributions of excited-state absorption were considered by virtue of the spin- and dipole-allowed triplet-triplet excitations within the fully equilibrated lowest triplet state structure (T_1, ^{3}MLCT), and the ground-state bleach was taken into account based on the dipole-allowed singlet-singlet transitions within the ground-state geometry. This computational approach was applied previously and is in particular suitable to characterize long-lived low-energy (triplet) states.[25] Several bright triplet-triplet excitations in Figure 4c and 4d, contributing to the excited-state absorption of $[Mo(L^{bi})_3]$ and $[Mo(L^{tri})_2]$, were investigated in more detail by means of TDDFT. The TA spectrum of $[Mo(L^{bi})_3]$ features a broad excited-state absorption band spanning from approximately 600 nm into the infrared region. This band can be attributed to an ^{3}ILCT within one of the bidentate ligands (T_{13} at 705 nm, 1.76 eV), whereas in $[Mo(L^{tri})_2]$ a mixed ^{3}LLCT with a slight ^{3}LMCT admixture is predicted by the quantum chemical simulations (T_{13} at 790 nm, 1.57 eV) in the same region. However, the band is not unambiguously detectable in the respective experimental spectrum. This ^{3}LMCT contribution may be involved in the deactivation of the excited species due to light-driven charge recombination in the vicinity of the metal center. Furthermore, the shoulder at around 500 nm observed for $[Mo(L^{bi})_3]$ is dominated by the five excited states: T_{26} and T_{30} (at 517 and 492 nm, 2.40 and 2.52 eV), which are both of mixed ^{3}LLCT and ^{3}MLCT nature, two excitations of mainly ^{3}LLCT character (T_{37} and T_{48}, at 463 and 433 nm, 2.68 and 2.86 eV) as well as into the T_{42} ^{3}LMCT state, which – again – is potentially involved in the deactivation of the excited species. Likewise, the respective shoulder observed in the TA spectrum of the tridentate complex, which seems to be mostly overshadowed by ground-state-bleach at approximately 500 nm, can be associated to the T_{40} (at 464 nm, 2.67 eV) of ^{3}MLCT character. Noteworthy, such ^{3}MLCT transitions may contribute to a further charge separation within the excited (triplet) state. Further details with respect to the simulated TA spectra as well as regarding the underlying electronic transitions are summarized in Tables S6 and S7.

For both Mo^0 complexes, the temporal evolution of all transient absorption signals is identical regardless of the detection wavelength and is furthermore identical to the emission decay (Figure 5). For instance, for $[Mo(L^{tri})_2]$, the decay of the excited-state absorption band at 390 nm (red trace in Figure 5b) is identical to the luminescence decay detected at 705 nm (green trace), and furthermore matches the ground-state bleach recoveries at 455 and 555 nm (black and blue traces) very well which is associated to S_5, S_6 and S_9 according to the performed simulations. Analogous observations are made for $[Mo(L^{bi})_3]$ in Figure 5a, indicating that there is a single photoactive excited state in both complexes. In deaerated THF at 20 °C all decay kinetics are single-exponential and ^{3}MLCT lifetimes of 18 and 19 ns are obtained (Table 1). In toluene under otherwise identical conditions, slower and bi-exponential excited-state decays are observable (Figure S3). Specifically, for

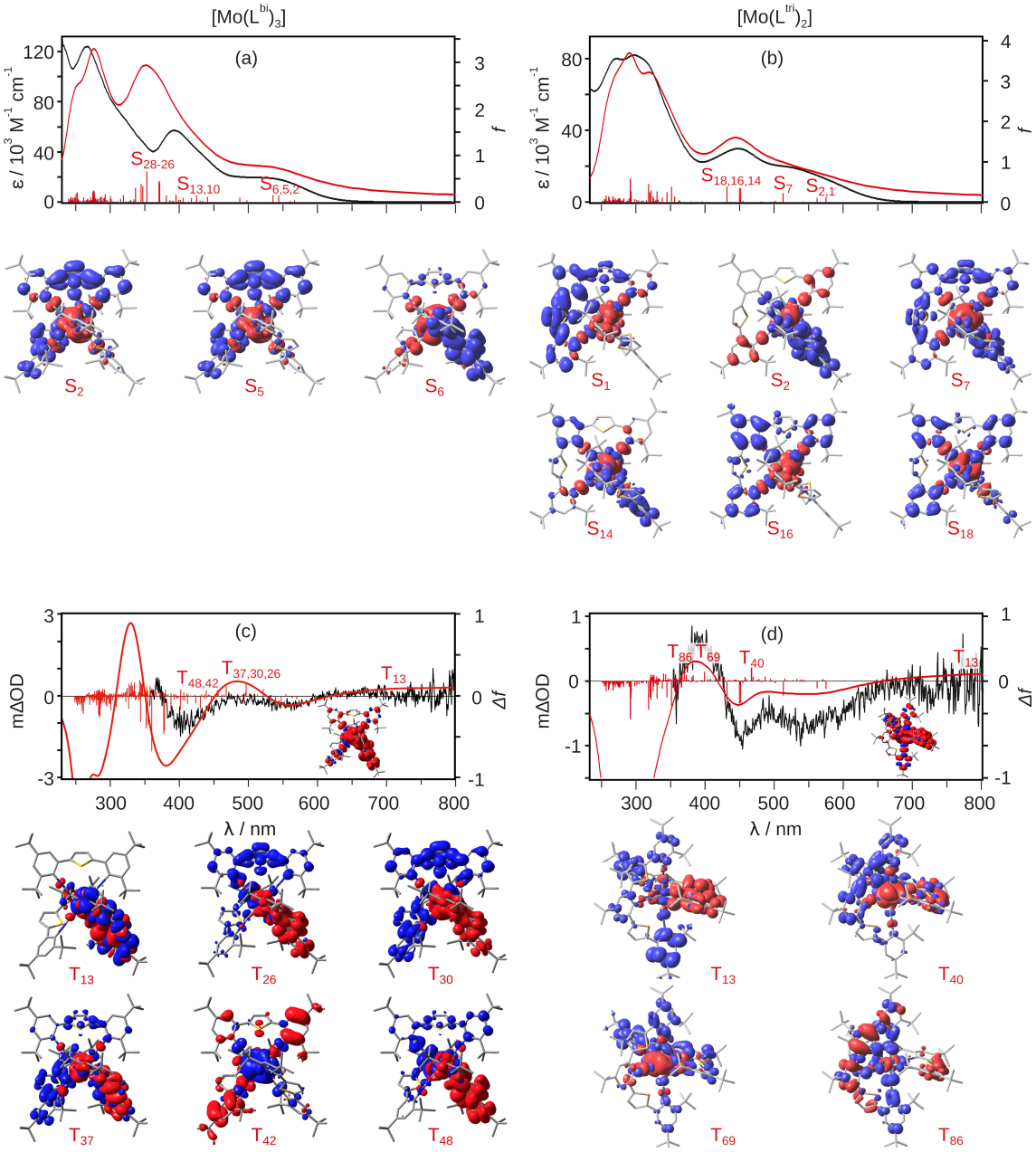

Figure 4. Comparison of experimental vs calculated UV/Vis and transient absorption data. Experimental UV/Vis absorption (black traces) of $[Mo(L^{bi})_3]$ (a) and $[Mo(L^{tri})_2]$ (b) in THF along with calculated spectra (red traces). Experimental transient difference spectra (black traces) of $[Mo(L^{bi})_3]$ (c) and $[Mo(L^{tri})_2]$ (d) in deaerated THF at 20 °C along with calculated difference spectra (red traces). Excitation for the transient UV/Vis measurements occurred at 620 nm with laser pulses of ca. 10 ns duration, spectra were time-integrated over a period of 200 ns following a time delay of 20 ns after excitation. Electronic transitions (red vertical bars), represent underlying dipole-allowed singlet–singlet and dipole-allowed triplet–triplet excitations, broadened by Lorentzian functions with a full width at half maximum of 0.25 eV. Spin densities are given for the respective lowest triplet states (T_1) as well as Charge Density Differences (CDDs) images for selected excitations. Excitations in the latter occur from red to blue.

$[Mo(L^{bi})_3]$ decay times of 30 and 83 ns with weighting factors of 73% and 27%, respectively, are obtained from a bi-exponential fit, whilst for $[Mo(L^{tri})_2]$ the decay times are 28 ns (62%) and 77 (38%), respectively (Table 1). The bi-exponential nature of the excited-state decays in toluene is attributed to slowly inter-converting conformers with somewhat different excited-state relaxation behavior. Depending on solvent, such bi-exponential decays were previously also observed for other Cr^0,[8a,b] Mn^I,[7a] and Mo^0 complexes[9] with comparable isocyanide chelate ligands. In particular, flipping of a bridging thiophene with respect to its two neighboring arylisocyanide units is presumed to lead to different conformers,[7a] and depending on the exact substituent patterns, the solvent and temperature, the inter-conversion between individual conformers can be faster or slower. In the present contribution, we estimate the driving force for such a flip of the thiophene moieties within the long-lived ^{3}MLCT equilibrium (T_1) to approximately 0.02 and to 0.01 eV in $[Mo(L^{bi})_3]$ and $[Mo(L^{tri})_2]$, respectively. In consequence,

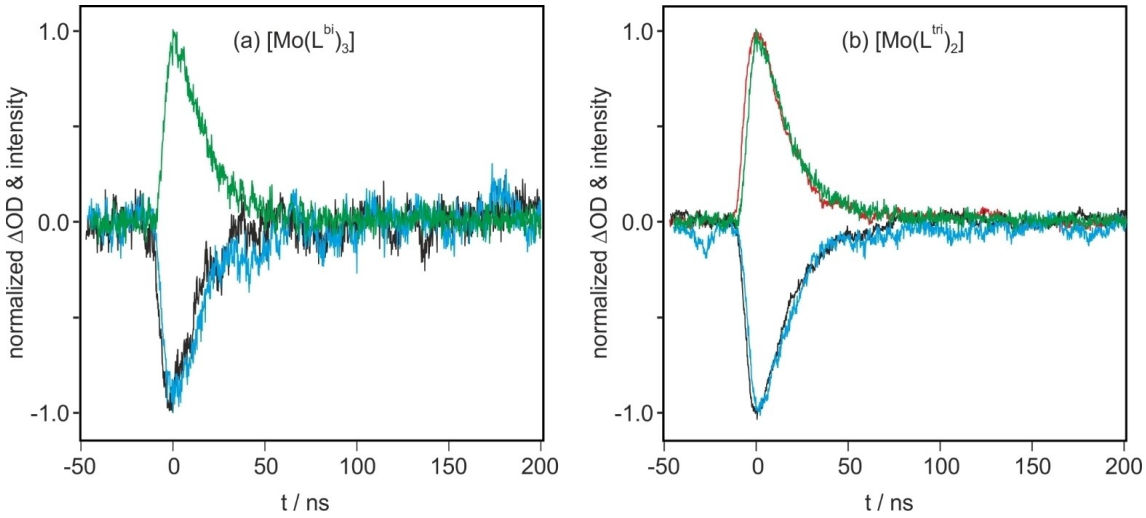

Figure 5. Temporal evolution of the photoluminescence intensity and the transient absorption difference signal at various detection wavelengths following pulsed excitation of (a) $[Mo(L^{bi})_3]$ and (b) $[Mo(L^{tri})_2]$ in deaerated THF at 20 °C. Excitation occurred at 620 nm with pulses of ca. 10 ns duration and energies of ca. 4 mJ. Luminescence decays (green traces) were detected at 705 nm, transient absorption bleach recoveries were monitored at 555 nm (blue traces) and at 400/455 nm (black traces), and the excited state absorption decay of $[Mo(L^{tri})_2]$ was followed at 390 nm (red trace).

rapid equilibration of both photoexcited isomers is in principle expected (Boltzmann factors for $Mo(L^{bi})_3]$ and $[Mo(L^{tri})_2]$ at 20 °C: 2.21 and 1.49, respectively). Though not physically completely correct, we will use weighted average lifetimes (τ_{avg}) to keep the forthcoming discussion simple. The fact that τ_{avg} is substantially longer for both complexes in toluene than the lifetimes in THF (44/47 ns vs 18/19 ns for $[Mo(L^{bi})_3]$/$[Mo(L^{tri})_2]$) is likely due to the increased ^{3}MLCT energy with decreased solvent polarity and consequent less efficient nonradiative relaxation from the ^{3}MLCT directly to the electronic ground state.

Excited-State Relaxation Pathways

In Ru^{II} polypyridines, thermally activated nonradiative relaxation from the emissive ^{3}MLCT state via an energetically nearby ^{3}MC state typically plays an important role (Figure 6b).[26,28] That ^{3}MC state is strongly distorted relative to the ^{3}MLCT and the electronic ground state (^{1}GS), leading to a relatively small activation barrier for internal conversion from the ^{3}MLCT to the ^{3}MC state, and from there onward relaxation to ^{1}GS.[5b,14,29] It seems plausible that the same relaxation pathway is also amenable in our isoelectronic Mo^0 complexes, and therefore we performed temperature-dependent luminescence lifetime studies (Figure 6a) to explore this aspect. Since the decay times

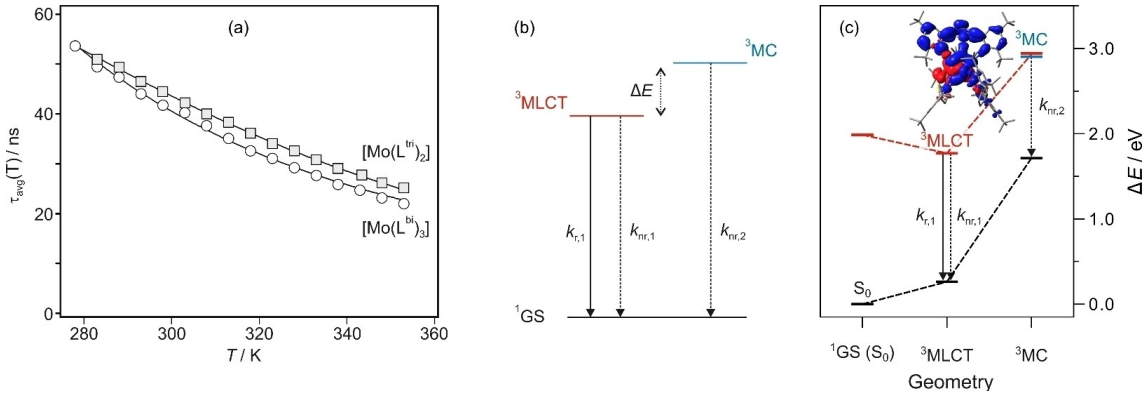

Figure 6. (a) Temperature-dependence of the (weighted average) luminescence lifetimes (τ_{avg}) of $[Mo(L^{bi})_3]$ (open circles) and $[Mo(L^{tri})_2]$ (gray filled squares) in deaerated toluene. The solid lines are fits with Equation (1) to the experimental data, yielding the parameters in Table 2.[26] (b) Deactivation of the ^{3}MLCT excited state (red) via direct radiative ($k_{r,1}$) and nonradiative ($k_{nr,1}$) relaxation to the electronic ground state (^{1}GS) and via thermal population of a metal-centered (^{3}MC, blue) excited state and subsequent nonradiative relaxation ($k_{nr,2}$). ΔE reflects an activation energy for internal conversion from the ^{3}MLCT to the ^{3}MC state, rather than a true energy difference between states. Equation (1) emerges from the three-level model in Figure 6b.[26] (c) Simulated excited-state relaxation pathways via radiative and nonradiative ^{3}MLCT decays as well as by nonradiative ^{3}MC decay as shown exemplarily for $[Mo(L^{bi})_3]$. All energies are shown within the fully optimized equilibrium structures of the involved singlet (S_0) and triplet states (^{3}MLCT and ^{3}MC). Electronic character of the ^{3}MC state of interest is indicated by a charge density difference (CDD); excitations occur from red to blue. Cartesian coordinates of simulated intermediates are provided in Ref. [27].

in toluene are longer, and since that solvent permits measurements over a greater temperature range than THF, toluene was the preferred choice despite the abovementioned conformer issue. τ_{avg} values as a function of temperature can be modelled using Equation (1), which describes the overall ^{3}MLCT decay as a function of radiative relaxation ($k_{r,1}$), direct nonradiative relaxation to the ground state ($k_{nr,1}$), and indirect nonradiative relaxation via thermal population of the ^{3}MC state ($k_{nr,2}$).[26] ΔE is the activation energy required to populate the ^{3}MC from the ^{3}MLCT state, and k_B is Boltzmann's constant.

$$\tau_{avg}(T) = [k_{r,1} + k_{nr,1} + k_{nr,2} \cdot \exp(-\Delta E/k_B \cdot T)]^{-1} \quad (1)$$

The solid lines in Figure 6a are the outcomes of three-parameter fits to the experimental data (open circles for $[Mo(L^{bi})_3]$, gray squares for $[Mo(L^{tri})_2]$), whereby the sum $k_{r,1} + k_{nr,1}$ was treated as a single fit parameter in addition to $k_{nr,2}$ and ΔE. This simplistic approach yields the parameters listed in Table 2. Though the obtained parameter values are undoubtedly associated with considerable uncertainty, it seems clear that ^{3}MLCT relaxation directly to the ground state occurs with total rate constants on the order of 10^6 to 10^7 s^{-1} (second column in Table 2), whereas relaxation from the ^{3}MC state is considerably faster (third column). The ^{3}MC state seems to be 0.11 – 0.16 eV above the ^{3}MLCT excited state in both $[Mo(L^{bi})_3]$ and $[Mo(L^{tri})_2]$ (fourth column). According to this analysis, the activation energy for ^{3}MLCT–^{3}MC internal conversion (ΔE) is roughly a factor of two to three smaller in these new Mo^0 complexes than in the previously explored $[Mo(L^{tBu})_3]$ compound and in $[Ru(bpy)_3]^{2+}$.[9,26, 30] Along with lowered ^{3}MLCT energy and the ensuing effect of the energy gap law, this can account for the much lower luminescence quantum yields of $[Mo(L^{bi})_3]$ and $[Mo(L^{tri})_2]$ (0.7 %, Table 1), compared to 20.3 % for $[Mo(L^{tBu})_3]$ under identical conditions in deaerated toluene at 20 °C. In order to address the competitive excited-state relaxation pathways, accessible upon 390-nm excitation at the molecular level, we fully optimized the involved triplet excited states, i.e., the lowest ^{3}MLCT as well as the lowest ^{3}MC of $[Mo(L^{bi})_3]$, $[Mo(L^{tri})_2]$ and $[Mo(L^{tBu})_3]$, respectively, by means of TDDFT and our recently introduced external optimizer that is also aware of excited states – pysisyphus.[31] These simulations reveal that of the six prominent ^{3}MC states, the lowest unrelaxed ^{3}MC state is predicted for all three Mo^0 complexes at an excitation energy exceeding 5 eV (below 250 nm) at the Franck-Condon point, and is thus not directly accessible. Therefore, these ^{3}MC states are determined to be significantly higher in energy (approximately +1.5 eV) than in isoelectronic Ru^{II} polypyridyl complexes as predicted at a similar computational level of theory.[29,32] In case of the present Mo^0 complexes with a d^6 configuration, this low-lying ^{3}MC state features one singly occupied t_{2g} orbital, i.e. d_π(421) and d_π(409) in $[Mo(L^{bi})_3]$ and $[Mo(L^{tri})_2]$, respectively, as well as one singly occupied e_g orbital, i.e. the respective d_{z^2} orbital; see Table S3. Upon population transfer via ultrafast intersystem crossing from the ^{1}MLCT state and internal conversion, the lowest ^{3}MLCT state (T_1) is populated, while only a slight stabilization of 0.22 and 0.19 eV is predicted in the case of the ^{3}MLCT from the singlet ground state structure for $[Mo(L^{bi})_3]$ and $[Mo(L^{tri})_2]$, respectively. This finding is not surprising, as only minor structural alternations are observed for these MLCT states. In a similar fashion, the ^{3}MLCT state of $[Mo(L^{tBu})_3]$ undergoes only minor stabilization of 0.16 eV upon equilibration from the Franck-Condon point. However, the ^{3}MC undergo substantial structural rearrangement, i.e., yielding the cleavage of one Mo–C bond along the *z*-axis due to the population of the d_{z^2} orbital (involved in the σ^*-backbonding), see Table S1 and Figures S3-S5. In consequence, the lowest ^{3}MC state of interest is stabilized from ~5 eV within the singlet ground state structure to 2.91 and 2.93 eV for $[Mo(L^{bi})_3]$ and $[Mo(L^{tri})_2]$, respectively, in the relaxed ^{3}MC states. In case of $[Mo(L^{tBu})_3]$, the respective ^{3}MC state is predicted at slightly lower energy (2.76 eV) in its fully relaxed equilibrium. Therefore, the computational modelling is qualitatively in agreement with the spectroscopic results, which indicate a thermally accessible ^{3}MC state – leading upon population to efficient radiationless deactivation as shown exemplarily for $[Mo(L^{bi})_3]$ in Figure 6c (see Figure S7 for $[Mo(L^{tri})_2]$). However, the calculated activation energy of approximately 1.1 eV for ^{3}MC population from the lowest ^{3}MLCT state is substantially higher than the experimentally determined value of merely 0.12 eV. It seems plausible that this deviation is due to dominant explicit solvent effects in the ^{3}MC equilibria. The respective molecular structures have one cleaved Mo–C bond, and the vacant coordination site at the metal center is presumably at least partially occupied by THF, thereby stabilizing the energy of the relevant ^{3}MC states further in their relaxed structures. Addressing explicit solvent effects for photoexcited intermediates is beyond the scope of the present study. Based on the simulated relaxation schemes, $[Mo(L^{bi})_3]$ and $[Mo(L^{tri})_2]$ would be estimated to feature enhanced excited-state lifetimes with respect to $[Mo(L^{tBu})_3]$ as evident from the relative energies of the deactivating ^{3}MC states – which is in contrast to the experimental observation. Likely, this contradiction can be understood in terms of the thiophene-flip discussed above, which could be an efficient dissipative sink, because each flip consumes approximately 0.01 – 0.02 eV for $[Mo(L^{bi})_3]$ and $[Mo(L^{tri})_2]$, respectively. In $[Mo(L^{tBu})_3]$, an analogous phenyl-flip is not possible due to the more rigid ligand frame (Table S1 and Figures S4-S6).

The key structural difference between the previously reported $[Mo(L^{tBu})_3]$ complex and the new Mo^0 isocyanides is

Table 2. Relaxation of the emissive ^{3}MLCT state directly to the ground state (^{1}GS) and via thermal population of a ^{3}MC state. The different radiative ($k_{r,1}$) and nonradiative rate constants ($k_{nr,1}$ and $k_{nr,2}$) are as defined in Figure 6b and were obtained from fits with Equation (1) to the temperature-dependent luminescence lifetime data in Figure 6a. ΔE is the activation energy for ^{3}MLCT – ^{3}MC internal conversion (Figure 6b).[26] λ_{em} is the emission band maximum.

compound	$k_{r,1} + k_{nr,1}$ [s^{-1}]	$k_{nr,2}$ [s^{-1}]	ΔE [eV]	λ_{em} [nm]
$[Mo(L^{bi})_3]$	$3.8 \cdot 10^6$	$1.7 \cdot 10^9$	0.11	728
$[Mo(L^{tri})_2]$	$12 \cdot 10^6$	$6.3 \cdot 10^9$	0.16	722
$[Mo(L^{tBu})_3]$[a]	$0.38 \cdot 10^6$	$360 \cdot 10^9$	0.36	583
$[Ru(bpy)_3]^{2+}$[b]	$1.3 \cdot 10^6$	$10000 \cdot 10^9$	0.44	622

[a] From Refs. [9, 30]. [b] from Ref. [26].

the presence of thiophene (instead of phenylene) bridging units in the ligand backbone. This change in ligand design therefore does not only induce a lowered ^{3}MLCT energy relative to the electronic ground state, but at the same time also lowers the barrier for internal conversion from the ^{3}MLCT to the ^{3}MC state, at least based on the experimental (temperature-dependent) emission results. Based on the emission band maxima in Table 1 and a λ_{em}-value of 583 nm for $[Mo(L^{tBu})_3]$,[9] the ^{3}MLCT energy decreases by approximately 0.37 eV between $[Mo(L^{tBu})_3]$ and the new Mo^0 complexes from Figure 1, whilst the activation energy for internal conversion from the ^{3}MLCT to the ^{3}MC state (ΔE) simultaneously decreases by roughly 0.25 eV. In principle, one could have expected that an energetic stabilization of the emissive ^{3}MLCT state will entail an increased activation energy for internal conversion to the ^{3}MC state, but evidently this is not the case. Instead, it seems that the ligands L^{bi} and L^{tri} impose a much weaker ligand field than L^{tBu} leading to a situation in which the distortion of the ^{3}MC state is substantially changed in such a way that ^{3}MLCT – ^{3}MC internal conversion is facilitated as suggested by the computational results. This finding is consistent with that of a recent study, in which we investigated another Mo^0 complex with isocyanide chelate ligands incorporating thiophene bridging units.[11] Additionally, the thiophene flip is likely an efficient energy sink lowering the ^{3}MLCT excited-state lifetime of the two Mo^0 complexes from Figure 1.

Conclusions

With their thiophene bridging units between arylisocyanide ligating units, L^{bi} and L^{tri} yield deep-red emitting homoleptic Mo^0 complexes whose photophysical properties resemble those of $[Os(bpy)_3]^{2+}$ and $[Os(tpy)_2]^{2+}$, whilst previously explored isocyanide chelate ligands with phenylene bridging units gave homoleptic Mo^0 complexes with luminescence behavior reminiscent of $[Ru(bpy)_3]^{2+}$.[9,10] Unfortunately, the energetic stabilization of the emissive ^{3}MLCT excited state causing the red-shifted photoluminescence does not only lead to the expectable increase in nonradiative relaxation following the energy gap law, but instead there is also enhanced indirect ^{3}MLCT relaxation via a nearby ^{3}MC state that is known to play a key role in Ru^{II} and Fe^{II} photophysics.[14b,33] This leads to modest luminescence quantum yields (below 1%) for Mo^0 complexes with isocyanide chelate ligands incorporating thiophene bridging units. Furthermore it seems plausible that excited-state energy dissipation takes place by the flip of the central thiophene moieties in the ligand architecture of $[Mo(L^{bi})_3]$ and $[Mo(L^{tri})_2]$, facilitating efficient nonradiative relaxation. Therefore, it could be interesting to explore ligand variants in which the bridging units between individual arylisocyanides are oxidized to thiophene sulfone,[34] because in that case the flipping motion would likely be impeded.

Alternative ligand designs for deep-red and near-infrared emitting complexes made from earth-abundant d^6 metals could aim to exploit delocalization effects to enhance the photoluminescence quantum yields.[3,8b] Studies of Ru^{II} and Os^{II} polypyridines demonstrated that increased delocalization of the MLCT-excited electron leads to weaker excited-state distortion, and thereby nonradiative relaxation is decelerated.[35] It seems plausible that such effects could also be exploitable for Mo^0 and related d^6 metal isocyanide compounds.

Acknowledgements

This work was supported by the Swiss National Science Foundation through grant number 200021_178760. Funding by the German Research Foundation (DFG) within the PHOTOACC project (project number KU 3933/2-1) is gratefully acknowledged. All calculations were performed at the Universitätsrechenzentrum of the Friedrich Schiller University Jena. Open access funding provided by Universität Basel.

Conflict of Interest

The authors declare no conflict of interest.

Data Availability Statement

The data that support the findings of this study are available in the supplementary material of this article.

Keywords: chelates · molybdenum · isocyanide ligands · quantum chemistry · time-resolved spectroscopy

[1] a) A. Juris, V. Balzani, F. Barigelletti, S. Campagna, P. Belser, A. Von Zelewsky, *Coord. Chem. Rev.* **1988**, *84*, 85–277; b) M. S. Lowry, S. Bernhard, *Chem. Eur. J.* **2006**, *12*, 7970–7977; c) A. F. Henwood, E. Zysman-Colman, *Top. Curr. Chem.* **2016**, *374*, 41; d) K. L. Smitten, P. A. Scattergood, C. Kiker, J. A. Thomas, P. I. P. Elliott, *Chem. Sci.* **2020**, *11*, 8928–8935; e) Y. Sasaki, N. Yanai, N. Kimizuka, *Inorg. Chem.* **2022**; f) J. M. Favale, E. O. Danilov, J. E. Yarnell, F. N. Castellano, *Inorg. Chem.* **2019**, *58*, 8750–8762; g) T. P. Nicholls, L. K. Burt, P. V. Simpson, M. Massi, A. C. Bissember, *Dalton Trans.* **2019**, *48*, 12749–12754.

[2] a) O. S. Wenger, *J. Am. Chem. Soc.* **2018**, *140*, 13522–13533; b) C. Förster, K. Heinze, *Chem. Soc. Rev.* **2020**, *49*, 1057–1070.

[3] C. Wegeberg, O. S. Wenger, *JACS Au* **2021**, *1*, 1860–1876.

[4] a) Y. Z. Liu, T. Harlang, S. E. Canton, P. Chabera, K. Suarez-Alcantara, A. Fleckhaus, D. A. Vithanage, E. Goransson, A. Corani, R. Lomoth, V. Sundström, K. Wärnmark, *Chem. Commun.* **2013**, *49*, 6412–6414; b) P. Chábera, K. S. Kjaer, O. Prakash, A. Honarfar, Y. Z. Liu, L. A. Fredin, T. C. B. Harlang, S. Lidin, J. Uhlig, V. Sundström, R. Lomoth, P. Persson, K. Wärnmark, *J. Phys. Chem. Lett.* **2018**, *9*, 459–463; c) T. Duchanois, T. Etienne, C. Cebrian, L. Liu, A. Monari, M. Beley, X. Assfeld, S. Haacke, P. C. Gros, *Eur. J. Inorg. Chem.* **2015**, 2469–2477; d) P. Zimmer, L. Burkhardt, A. Friedrich, J. Steube, A. Neuba, R. Schepper, P. Müller, U. Florke, M. Huber, S. Lochbrunner, M. Bauer, *Inorg. Chem.* **2018**, *57*, 360–373; e) J. D. Braun, I. B. Lozada, C. Kolodziej, C. Burda, K. M. E. Newman, J. van Lierop, R. L. Davis, D. E. Herbert, *Nat. Chem.* **2019**, *11*, 1144–1150; f) S. M. Fatur, S. G. Shepard, R. F. Higgins, M. P. Shores, N. H. Damrauer, *J. Am. Chem. Soc.* **2017**, *139*, 4493–4505; g) S. S. Nair, O. A. Bysewski, S. Kupfer, M. Wächtler, A. Winter, U. S. Schubert, B. Dietzek, *Inorg. Chem.* **2021**, *60*, 9157–9173; h) T. Duchanois, L. Liu, M. Pastore, A. Monari, C. Cebrian, Y. Trolez, M. Darari, K. Magra, A. Frances-Monerris, E. Domenichini, M. Beley, X. Assfeld, S. Haacke, P. C. Gros, *Inorganics* **2018**, *6*, 63; i) M. Wächtler, J. Kübel, K. Barthelmes, A. Winter, A. Schmiedel, T. Pascher, C. Lambert, U. S. Schubert, B. Dietzek, *Phys. Chem. Chem. Phys.*

2016, *18*, 2350–2360; j) T. Jiang, Y. Bai, P. Zhang, Q. Han, D. B. Mitzi, M. J. Therien, *Proc. Natl. Acad. Sci. USA* **2020**, *117*, 20430–20437.
[5] a) J. K. McCusker, *Science* **2019**, *363*, 484–488; b) O. S. Wenger, *Chem. Eur. J.* **2019**, *25*, 6043–6052; c) W. Leis, M. A. Argüello Cordero, S. Lochbrunner, H. Schubert, A. Berkefeld, *J. Am. Chem. Soc.* **2022**, *144*, 1169–1173.
[6] a) M. D. Woodhouse, J. K. McCusker, *J. Am. Chem. Soc.* **2020**, *142*, 16229–16233; b) S. Parisien-Collette, A. C. Hernandez-Perez, S. K. Collins, *Org. Lett.* **2016**, *18*, 4994–4997; c) A. Gualandi, M. Marchini, L. Mengozzi, M. Natali, M. Lucarini, P. Ceroni, P. G. Cozzi, *ACS Catal.* **2015**, *5*, 5927–5931; d) W.-J. Zhou, X.-D. Wu, M. Miao, Z.-H. Wang, L. Chen, S.-Y. Shan, G.-M. Cao, D.-G. Yu, *Chem. Eur. J.* **2020**, *26*, 15052–15064.
[7] a) P. Herr, C. Kerzig, C. B. Larsen, D. Häussinger, O. S. Wenger, *Nat. Chem.* **2021**, *13*, 956–962; b) C. Wegeberg, O. S. Wenger, *Dalton Trans.* **2022**, *51*, 1297–1302.
[8] a) L. A. Büldt, X. Guo, R. Vogel, A. Prescimone, O. S. Wenger, *J. Am. Chem. Soc.* **2017**, *139*, 985–992; b) C. Wegeberg, D. Häussinger, O. S. Wenger, *J. Am. Chem. Soc.* **2021**, *143*, 15800–15811.
[9] P. Herr, F. Glaser, L. A. Büldt, C. B. Larsen, O. S. Wenger, *J. Am. Chem. Soc.* **2019**, *141*, 14394–14402.
[10] a) L. A. Büldt, X. Guo, A. Prescimone, O. S. Wenger, *Angew. Chem. Int. Ed.* **2016**, *55*, 11247–11250; *Angew. Chem.* **2016**, *128*, 11413–11417; b) L. A. Büldt, O. S. Wenger, *Dalton Trans.* **2017**, *46*, 15175–15177; c) L. A. Büldt, O. S. Wenger, *Angew. Chem. Int. Ed.* **2017**, *56*, 5676–5682; *Angew. Chem.* **2017**, *129*, 5770–5776.
[11] J. B. Bilger, C. Kerzig, C. B. Larsen, O. S. Wenger, *J. Am. Chem. Soc.* **2021**, *143*, 1651–1663.
[12] J. V. Caspar, T. J. Meyer, *J. Phys. Chem.* **1983**, *87*, 952–957.
[13] E. A. Medlycott, G. S. Hanan, *Chem. Soc. Rev.* **2005**, *34*, 133–142.
[14] a) Y. Z. Liu, P. Persson, V. Sundström, K. Wärnmark, *Acc. Chem. Res.* **2016**, *49*, 1477–1485; b) W. K. Zhang, K. J. Gaffney, *Acc. Chem. Res.* **2015**, *48*, 1140–1148.
[15] a) R. Hamze, J. L. Peltier, D. Sylvinson, M. Jung, J. Cardenas, R. Haiges, M. Soleilhavoup, R. Jazzar, P. I. Djurovich, G. Bertrand, M. E. Thompson, *Science* **2019**, *363*, 601–606; b) S. Shi, M. C. Jung, C. Coburn, A. Tadle, D. Sylvinson, P. I. Djurovich, S. R. Forrest, M. E. Thompson, *J. Am. Chem. Soc.* **2019**, *141*, 3576–3588; c) M. Gernert, L. Balles-Wolf, F. Kerner, U. Müller, A. Schmiedel, M. Holzapfel, C. M. Marian, J. Pflaum, C. Lambert, A. Steffen, *J. Am. Chem. Soc.* **2020**, *142*, 8897–8909; d) M. S. Lazorski, F. N. Castellano, *Polyhedron* **2014**, *82*, 57–70.
[16] a) Y. Zhang, T. S. Lee, J. L. Petersen, C. Milsmann, *J. Am. Chem. Soc.* **2018**, *140*, 5934–5947; b) Y. Zhang, T. S. Lee, J. M. Favale, D. C. Leary, J. L. Petersen, G. D. Scholes, F. N. Castellano, C. Milsmann, *Nat. Chem.* **2020**, *12*, 345–352; c) O. S. Wenger, *Nat. Chem.* **2020**, *12*, 323–324.
[17] a) F. Reichenauer, C. Wang, C. Förster, P. Boden, N. Ugur, R. Báez-Cruz, J. Kalmbach, L. Carrella, E. Rentschler, C. Ramanan, G. Niedner-Schatteburg, M. Gerhards, M. Seitz, U. Resch-Genger, K. Heinze, *J. Am. Chem. Soc.* **2021**, *143*, 11843–11855; b) W. R. Kitzmann, J. Moll, K. Heinze, *Photochem. Photobiol. Sci.* **2022**; c) S. Otto, M. Dorn, C. Förster, M. Bauer, M. Seitz, K. Heinze, *Coord. Chem. Rev.* **2018**, *359*, 102–111.
[18] a) H. U. Kim, S. Sohn, W. Choi, M. Kim, S. U. Ryu, T. Park, S. Jung, K. S. Bejoymohandas, *J. Mater. Chem. C* **2018**, *6*, 10640–10658; b) S. Cerfontaine, S. A. M. Wehlin, B. Elias, L. Troian-Gautier, *J. Am. Chem. Soc.* **2020**, *142*, 5549–5555; c) M. Dorn, J. Kalmbach, P. Boden, A. Kruse, C. Dab, C. Reber, G. Niedner-Schatteburg, S. Lochbrunner, M. Gerhards, M. Seitz, K. Heinze, *Chem. Sci.* **2021**, *12*, 10780–10790; d) N. Sinha, J. R. Jiménez, B. Pfund, A. Prescimone, C. Piguet, O. S. Wenger, *Angew. Chem. Int. Ed.* **2021**, *60*, 23722–23728; e) C. A. Barker, X. S. Zeng, S. Bettington, A. S. Batsanov, M. R. Bryce, A. Beeby, *Chem. Eur. J.* **2007**, *13*, 6710–6717; f) A. Breivogel, M. Park, D. Lee, S. Klassen, A. Kuhnle, C. Lee, K. Char, K. Heinze, *Eur. J. Inorg. Chem.* **2014**, *2014*, 288–295; g) G. Cheng, Q. Y. Wan, W. H. Ang, C. L. Kwong, W. P. To, P. K. Chow, C. C. Kwok, C. M. Che, *Adv. Opt. Mater.* **2019**, *7*; h) D. H. Kim, A. D'Aleo, X. K. Chen, A. D. S. Sandanayaka, D. D. Yao, L. Zhao, T. Komino, E. Zaborova, G. Canard, Y. Tsuchiya, E. Choi, J. W. Wu, F. Fages, J. L. Bredas, J. C. Ribierre, C. Adachi, *Nature Photon.* **2018**, *12*, 98–104; i) A. Barbieri, E. Bandini, F. Monti, V. K. Praveen, N. Armaroli, *Top. Curr. Chem.* **2016**, *374*; j) A. K. Pal, D. B. Cordes, A. M. Z. Slawin, C. Momblona, A. Pertegas, E. Orti, H. J. Bolink, E. Zysman-Colman, *RSC Adv.* **2017**, *7*, 31833–31837.
[19] A. Schwab, 22.02.2022 ed., Friedrich-Schiller-Universität Jena, **2022**, p. 10.5281/zenodo.6226450.
[20] a) D. D. Klendworth, W. W. Welters, R. A. Walton, *Organometallics* **1982**, *1*, 336–343; b) T. B. Ditri, A. E. Carpenter, D. S. Ripatti, C. E. Moore, A. L. Rheingold, J. S. Figueroa, *Inorg. Chem.* **2013**, *52*, 13216–13229; c) K. R. Mann, M. Cimolino, G. L. Geoffroy, G. S. Hammond, A. A. Orio, G. Albertin, H. B. Gray, *Inorg. Chim. Acta* **1976**, *16*, 97–101; d) R. B. King, M. S. Saran, *Inorg. Chem.* **1974**, *13*, 74–78.
[21] M. J. Drance, J. D. Sears, A. M. Mrse, C. E. Moore, A. L. Rheingold, M. L. Neidig, J. S. Figueroa, *Science* **2019**, *363*, 1203–1205.
[22] L. J. Lyons, S. L. Pitz, D. C. Boyd, *Inorg. Chem.* **1995**, *34*, 316–322.
[23] C. K. Prier, D. A. Rankic, D. W. C. MacMillan, *Chem. Rev.* **2013**, *113*, 5322–5363.
[24] K. Suzuki, A. Kobayashi, S. Kaneko, K. Takehira, T. Yoshihara, H. Ishida, Y. Shiina, S. Oishic, S. Tobita, *Phys. Chem. Chem. Phys.* **2009**, *11*, 9850–9860.
[25] a) G. E. Shillito, T. B. J. Hall, D. Preston, P. Traber, L. Wu, K. E. A. Reynolds, R. Horvath, X. Z. Sun, N. T. Lucas, J. D. Crowley, M. W. George, S. Kupfer, K. C. Gordon, *J. Am. Chem. Soc.* **2018**, *140*, 4534–4542; b) L. Zedler, A. K. Mengele, K. M. Ziems, Y. Zhang, M. Wächtler, S. Gräfe, T. Pascher, S. Rau, S. Kupfer, B. Dietzek, *Angew. Chem. Int. Ed.* **2019**, *58*, 13140–13148; *Angew. Chem.* **2019**, *131*, 13274–13282; c) P. Buday, C. Kasahara, E. Hofmeister, D. Kowalczyk, M. K. Farh, S. Riediger, M. Schulz, M. Wächtler, S. Furukawa, M. Saito, D. Ziegenbalg, S. Gräfe, P. Bäuerle, S. Kupfer, B. Dietzek-Ivanšić, W. Weigand, *Angew. Chem. Int. Ed.* **2022**, doi: 10.1002/anie.202202079.
[26] J. Van Houten, R. J. Watts, *J. Am. Chem. Soc.* **1976**, *98*, 4853–4858.
[27] A. Schwab, 07.04.2022 ed., Friedrich-Schiller-Universität Jena, **2022**, p. 10.5281/zenodo.6420693.
[28] a) N. H. Damrauer, T. R. Boussie, M. Devenney, J. K. McCusker, *J. Am. Chem. Soc.* **1997**, *119*, 8253–8268; b) Q. C. Sun, B. Dereka, E. Vauthey, L. M. L. Daku, A. Hauser, *Chem. Sci.* **2017**, *8*, 223–230.
[29] A. Koch, D. Kinzel, F. Dröge, S. Gräfe, S. Kupfer, *J. Phys. Chem. C* **2017**, *121*, 16066–16078.
[30] P. Herr, O. S. Wenger, *Inorganics* **2020**, *8*, 14.
[31] J. Steinmetzer, S. Kupfer, S. Gräfe, *Int. J. Quantum Chem.* **2021**, *121*, e26390.
[32] S. Kupfer, M. Wächtler, J. Guthmuller, *ChemPhotoChem* **2022**, *6*, e202200010.
[33] a) A. Soupart, F. Alary, J. L. Heully, P. I. P. Elliott, I. M. Dixon, *Coord. Chem. Rev.* **2020**, *408*, 10; b) J. K. McCusker, K. N. Walda, R. C. Dunn, J. D. Simon, D. Magde, D. N. Hendrickson, *J. Am. Chem. Soc.* **1993**, *115*, 298–307.
[34] a) S. Tian, H. Ma, X. Wang, A. Lv, H. Shi, Y. Geng, J. Li, F. Liang, Z.-M. Su, Z. An, W. Huang, *Angew. Chem. Int. Ed.* **2019**, *58*, 6645–6649; *Angew. Chem.* **2019**, *131*, 6717–6721; b) P. R. Christensen, J. K. Nagle, A. Bhatti, M. O. Wolf, *J. Am. Chem. Soc.* **2013**, *135*, 8109–8112.
[35] a) J. A. Treadway, G. F. Strouse, R. R. Ruminski, T. J. Meyer, *Inorg. Chem.* **2001**, *40*, 4508–4509; b) J. A. Treadway, B. Loeb, R. Lopez, P. A. Anderson, F. R. Keene, T. J. Meyer, *Inorg. Chem.* **1996**, *35*, 2242–2246.

Manuscript received: February 24, 2022
Revised manuscript received: April 8, 2022
Accepted manuscript online: April 20, 2022
Version of record online: May 12, 2022